Electronic Supplementary Material (ESI) for Journal of Materials Chemistry B.

Engineering Proton Conductivity in Melanin Using Metal Doping

A. Bernardus Mostert, Shermiyah B. Rienecker, Margarita Sheliakina, Paul Zierep, Graeme R. Hanson, Jeffrey R. Harmer, Gerhard Schenk, Paul Meredith*

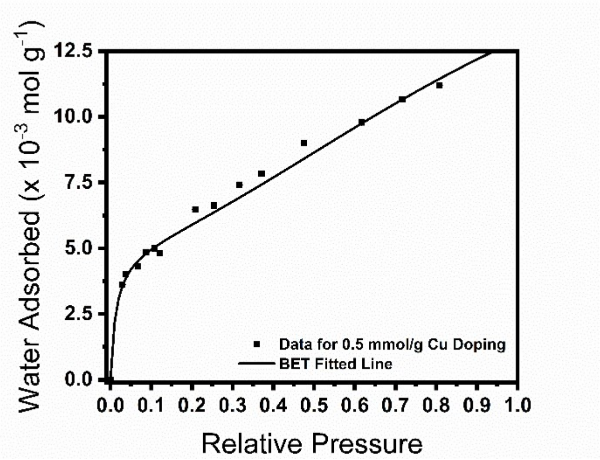

Figure S1. An adsorption isotherm of 0.5 mmol g^{-1} Cu-melanin using H_2O as the adsorbate. The solid line indicates the line of best fit from a limited layer BET isotherm.[S1] Parameters for the fit are found in **Table S1**. Method for obtaining the data is in the **Supplementary Methods**.

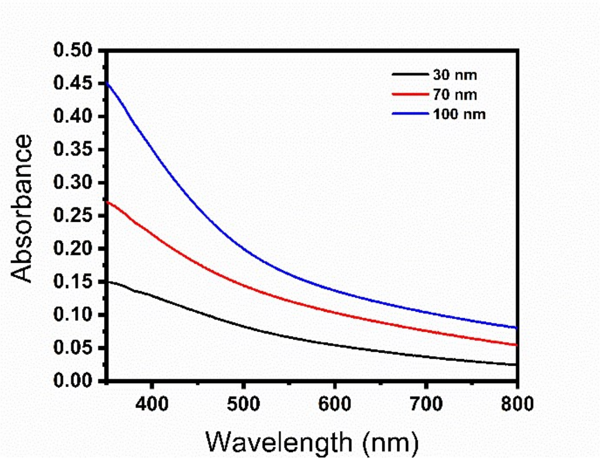

Figure S2. The UV-visible absorption spectra of melanin thin films. Thicknesses are indicated. The data is similar to melanin solutions.[S2] See Supplementary Methods for experimental details.

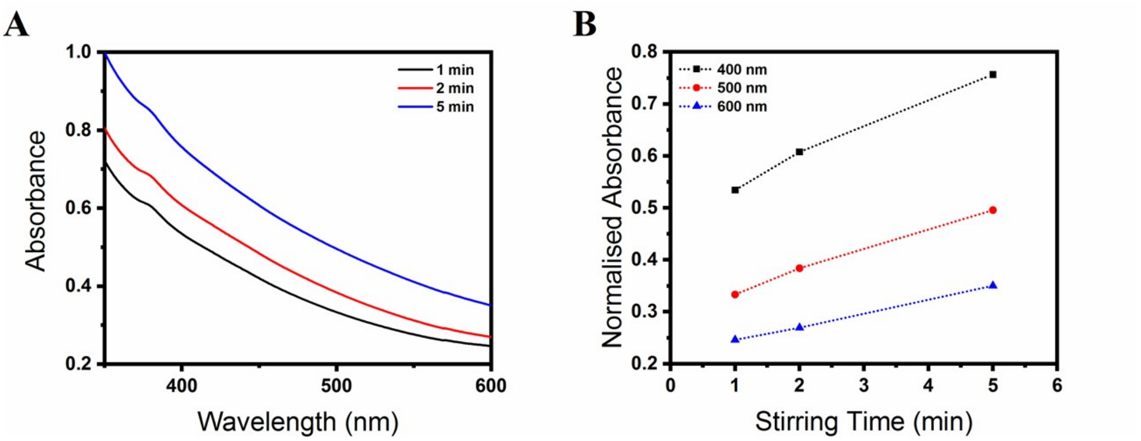

Figure S3. A) The UV-visible absorption spectra of Cu-melanin thin films for samples. Time after Cu(II) addition indicated (see Experimental Section). Thicknesses for the films were for the 1 min sample 70 nm, 2 min sample 190 nm and 5 min sample 1080 nm. The spectra is similar to Figure S2, indicating that it is a melanin like material. B) The normalized absorption as a function of stirring time (film thickness) for different wavelengths, which indicates that the change in the absorbance is due to an increasing absorption length. See Supplementary Methods for experimental details.

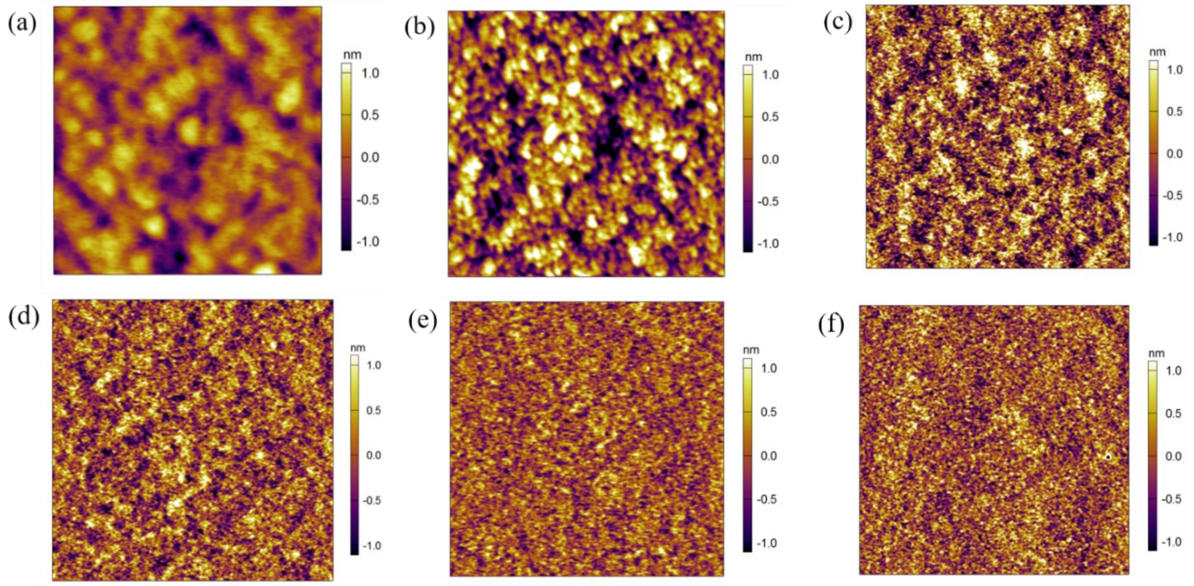

Figure S4. Topographic AFM images of a melanin thin film on a glass substrate taken at different image dimensions/magnifications: (a) 500 × 500 nm^2, (b) 1 × 1 µm^2, (c) 5 × 5 µm^2, (d) 10 × 10 µm^2, (e) 20 × 20 µm^2, (f) 30 × 30 µm^2. See Supplementary Methods for experimental details and supplementary discussion.

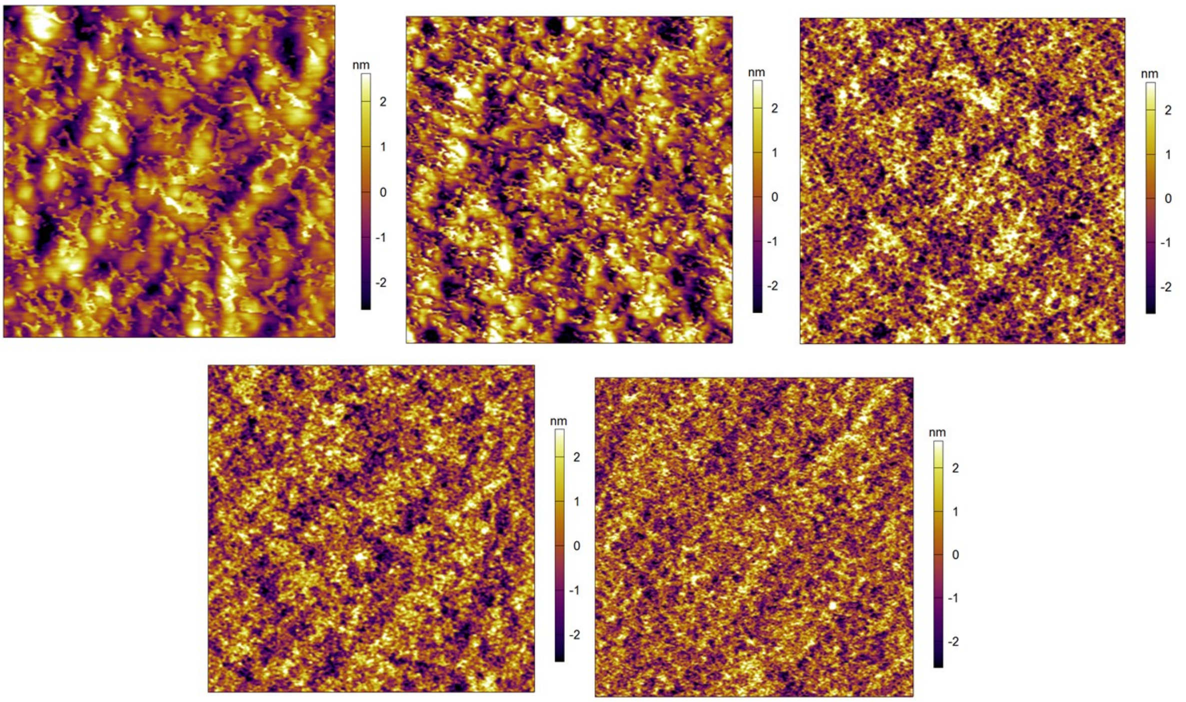

Figure S5. Topographic AFM images of a Cu-melanin thin film (spin coated 2 min after Cu addition) on a glass substrate taken at different image dimensions/magnifications: (a) 500 × 500 nm^2, (b) 1 × 1 µm^2, (c) 5 × 5 µm^2, (d) 10 × 10 µm^2, (e) 20 × 20 µm^2. For experimental details see Supplementary Methods.

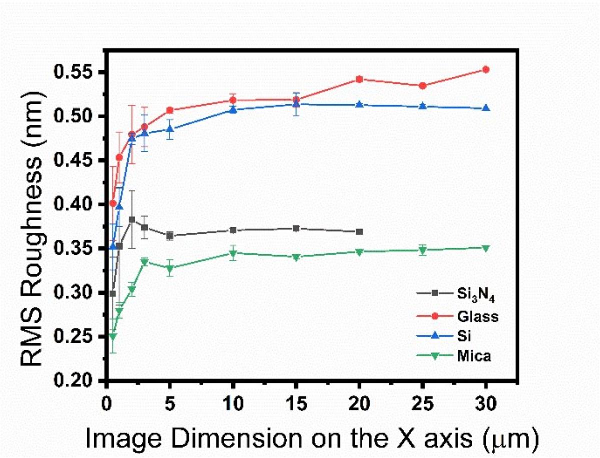

Figure S6. The root-mean-square (RMS) roughness as a function of image size for 50 nm melanin thin films spin-coated on different substrates. The data indicates that the films do not exceed a roughness of greater than 1 nm, which make the films excellent candidates for device applications. The uncertainties presented on the graph were calculated (2SE) across three different samples. See Supplementary Methods for experimental details.

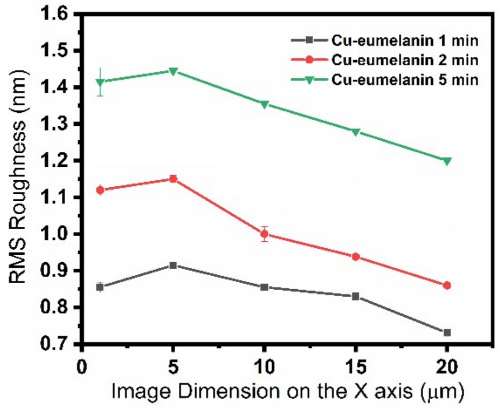

Figure S7. RMS roughness as a function of image size for different thickness (stirring time) of Cu-melanin thin films. The data indicates that the films do not exceed a roughness of greater than 2 nm. The uncertainties presented on the graph were calculated (2SE) across three different samples.

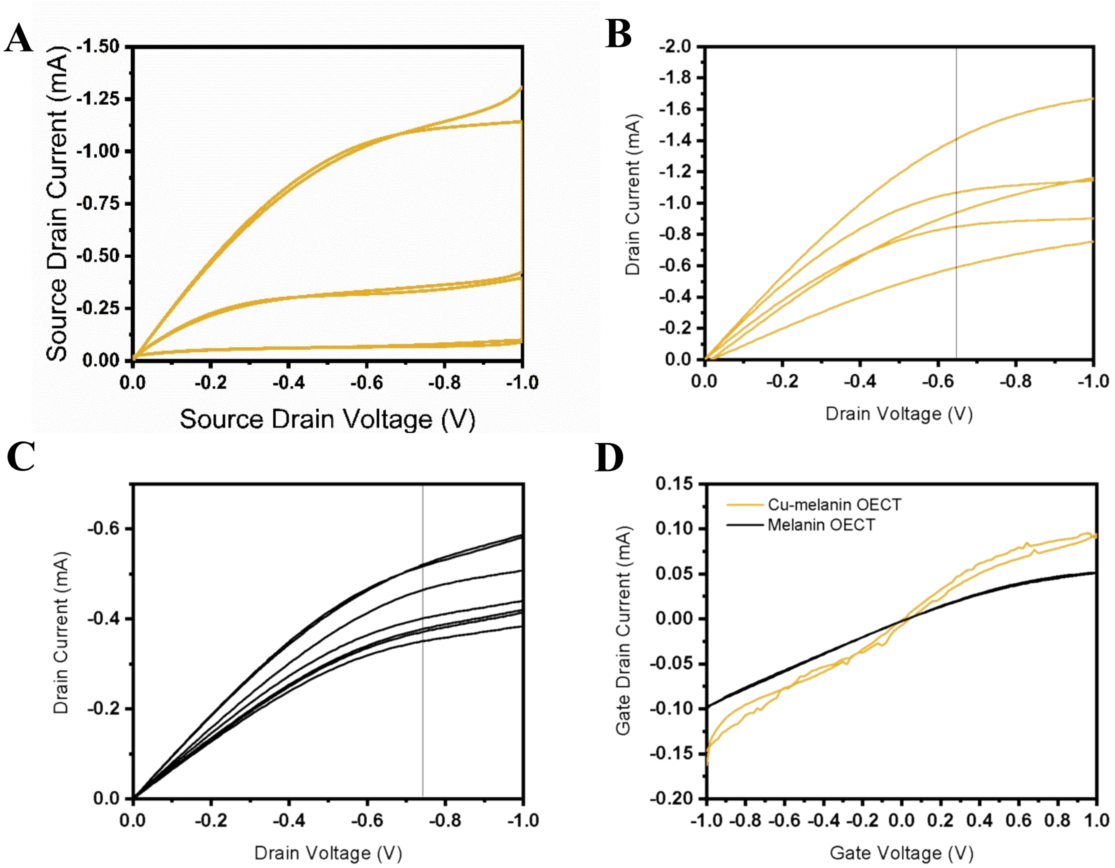

Figure S8. A) Example output characteristic of a Cu-melanin/PEDOT:PSS based OECT devices. Top curves are forward and backward sweeps at gate voltage = 0 V, middle set of curves for gate voltage = 0.4 V and bottom curves for gate voltage = 0.8 V. Delay time 5 s and hold time 60 s. B) The viable output curves (n = 5) for Cu-melanin OECTs at 0 V gate voltage in reverse scan. The potential range of pinch off voltages are from ~0.65 V upwards. C) The viable output curves (n=9) for neat melanin OECTs at 0 V gate voltage in reverse scan. The potential range of pinch off voltages are from ~0.75 V upwards. D) The leakage currents for the devices depicted in Figure 3. When inspecting B & C, one could anticipate that with an increase in proton concentration between the devices that the pinch off voltage could potentially move lower with increasing proton concentration. This may indeed be occurring if one compares B & C. However, the variation is too large to make such a definitive statement. This aspects of solid state OECTs should be explored in future research. Regarding D, the data are examples demonstrating that the Cu-melanin OECTs have a higher leakage current relative to the neat melanin OECTs. With further analysis, we determined the sizes of the leakage current at -1V and 1V for the device. It was found that for Cu-melanin OECTs the currents were $(-5.9\pm 3.0)\times10^{-4}$A and $(4.8\pm 2.3)\times10^{-4}$A respectively. Note uncertainties are to 2 times standard error. For neat melanin OECTs we found for -1V and 1V the leakage currents to be $(-1.82\pm 1.3)\times10^{-4}$A and $(1.7\pm 1.4)\times10^{-4}$A respectively. As can be seen from the size of the leakage currents, the Cu-melanin OECTs generate more current relative to the neat melanin OECTs. The different sizes of the leakage currents are entirely consistent with more mobile charges, i.e. protons, being present within the Cu-melanin OECTs vs the neat melanin OECTs.

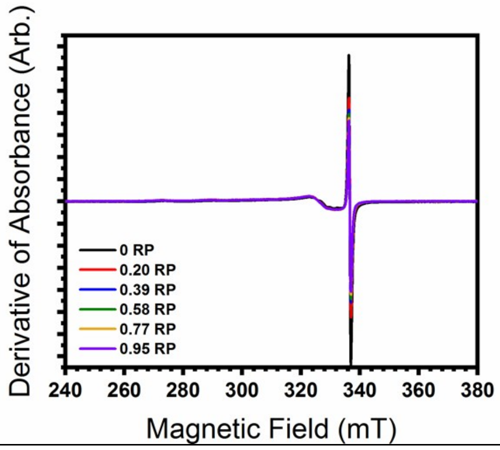

Figure S9. X-band CW-EPR spectra for Cu-melanin (0.05 mmol g^{-1} loading) upon which Figure 4 is based. The different curves were obtained at different vapor pressures as indicated in the legend (RP = Relative Pressure). See Experimental Section for experimental details.

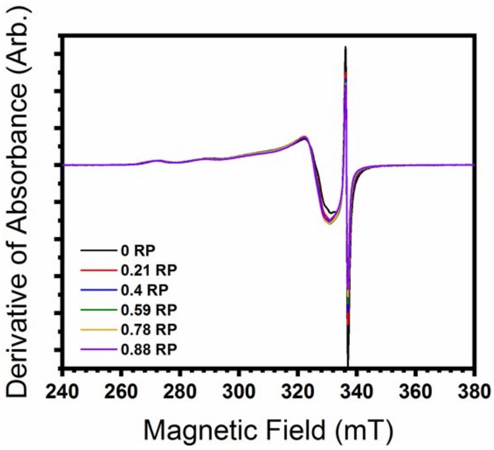

Figure S10. X-band CW-EPR spectra for Cu-melanin (0.1 mmol g^{-1} loading) upon which Figure 4 is based. The different curves were obtained at different vapor pressures as indicated in the legend (RP = Relative Pressure). See Experimental Section for experimental details.

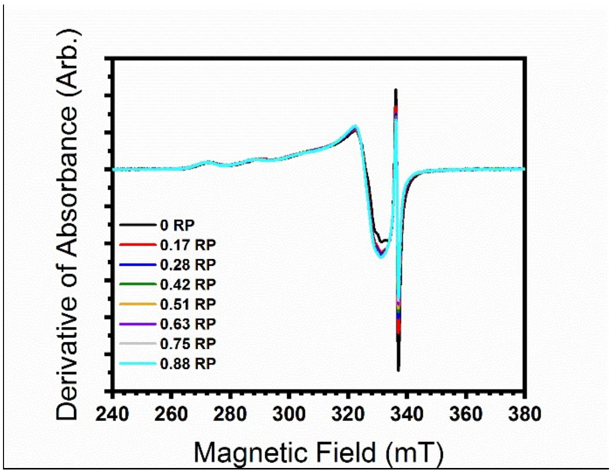

Figure S11. X-band CW-EPR spectra for Cu-melanin (0.25 mmol g^{-1} loading) upon which Figure 4 is based. The different curves were obtained at different vapor pressures as indicated in the legend (RP = Relative Pressure). See Experimental Section for experimental details.

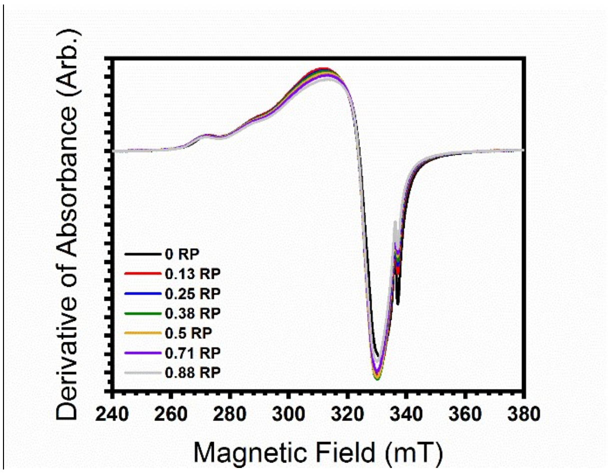

Figure S12. X-band CW-EPR spectra for Cu-melanin (0.5 mmol g^{-1} loading) upon which Figure 4 is based. The different curves were obtained at different vapor pressures as indicated in the legend (RP = Relative Pressure). See Experimental Section for experimental details.

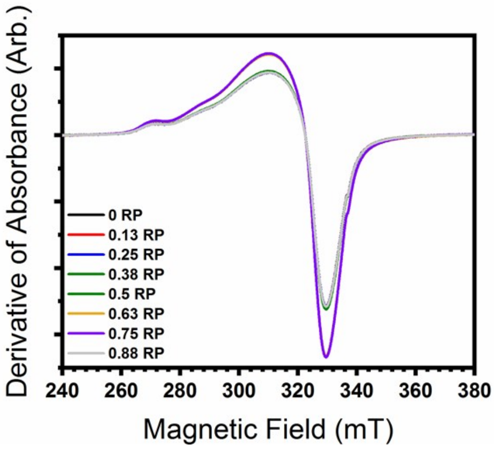

Figure S13. X-band CW-EPR spectra for Cu-melanin (1.0 mmol g^{-1} loading) upon which Figure 4 is based. The different curves were obtained at different vapor pressures as indicated in the legend (RP = Relative Pressure). See Experimental Section for experimental details.

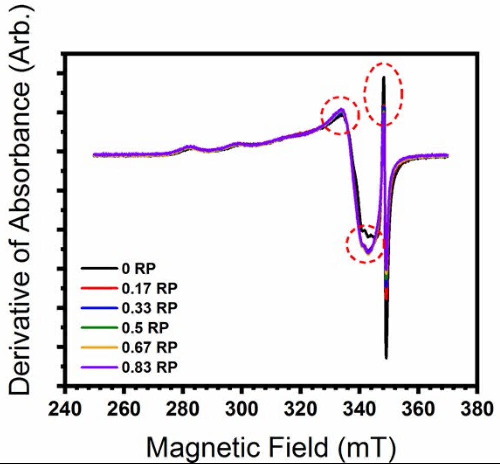

Figure S14. X-band CW-EPR spectra for Cu-melanin pellets with 0.25 mmol g^{-1} Cu(II) loading upon which Figure 4 is based. The different curves were obtained at different vapor pressures as indicated in the legend (RP = Relative Pressure). Shown here are the peaks on which time dependent photo EPR data was taken. See Experimental Section for experimental details.

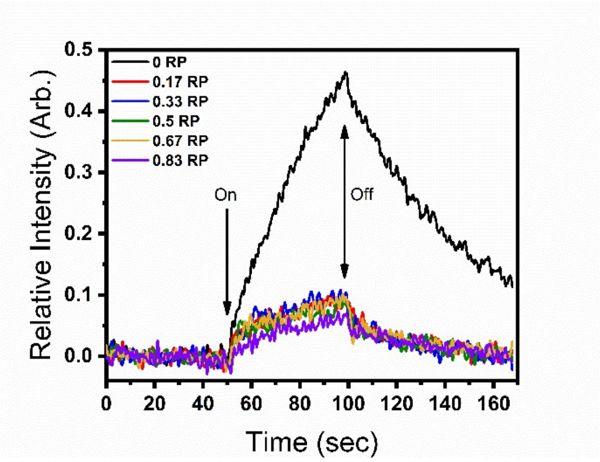

Figure S15. Photo-EPR signals for a Cu-melanin sample (0.25 mmol g^{-1} loading). Relative changes in CW-EPR signal intensity are shown here for the melanin peak. Colors indicate different relative pressures. See Supplementary Methods and discussion for more details.

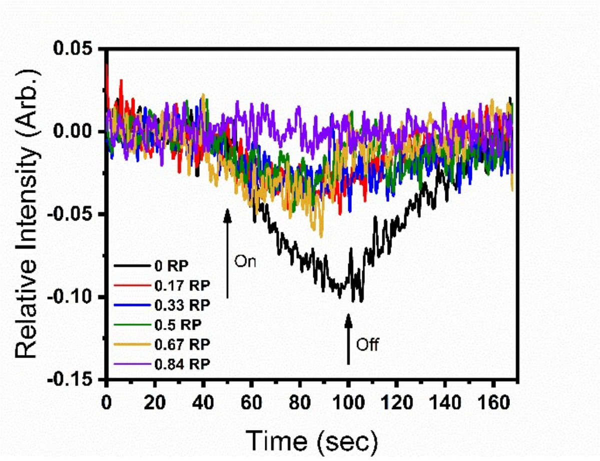

Figure S16. Photo-EPR signals for a Cu-melanin sample (0.25 mmol g^{-1}). Relative changes in CW-EPR signal intensity are shown here for the Cu(II) ⊥ peak component. Colors indicate different relative pressures. See Supplementary Methods and discussion for more details.

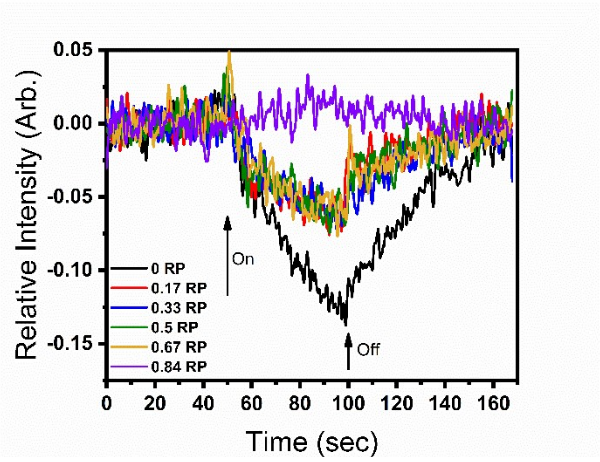

Figure S17. Photo-EPR signals for a Cu-melanin sample (0.25 mmol g^{-1} loading). Relative changes in CW-EPR signal intensity are shown here for the Cu(II) ⊥ dip (after applying the modulus/multiplying by -1). Colors indicate different relative pressures. See Supplementary Methods and discussion for more details.

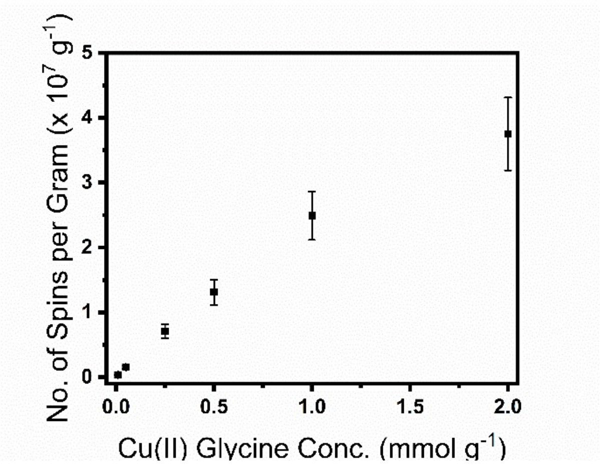

Figure S18. CW-EPR calibration curve for Cu(II) content using Cu-doped glycine powders (see Supplementary Methods). The number of spins derived from the CW-EPR spectra are plotted as a function of the amount of Cu(II) added to the glycine. The number of spins measured is linearly proportional to the Cu(II) concentration used except at very high Cu(II) content. Note that we did not study any sample at 2.0 mmol g^{-1}.

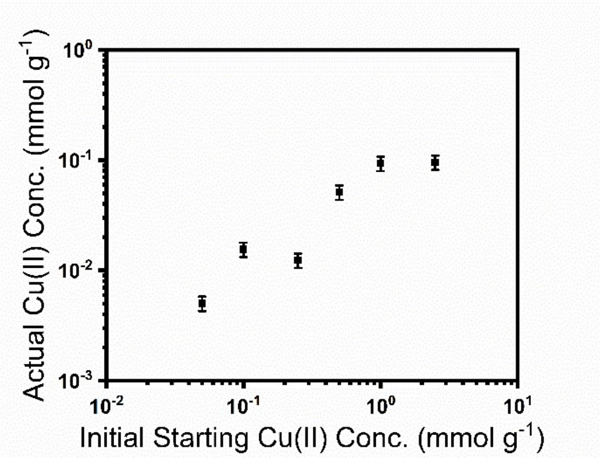

Figure S19. Concentration of Cu(II) in Cu-melanin powders. The final Cu(II) concentration (determined from the standard calibration curve in Figure S20) was an order of magnitude less than the starting Cu(II) concentration.

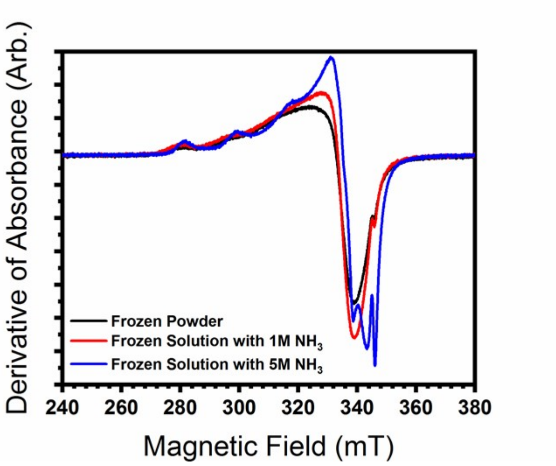

Figure S20. X-band CW-EPR spectra of Cu-melanin powder made with 0.5 mmol g^{-1} (black), with 1 M NH_3 (red), and 5 M NH_3 (blue). Measurements were performed at 130 K, 20 mW microwave power, and 0.0754 mT modulation amplitude. The increase in Cu(II) signal intensity is attributed to an increase in Cu(II) due to oxidation of Cu(I) present in the sample. See Supplementary Methods and discussion for more details.

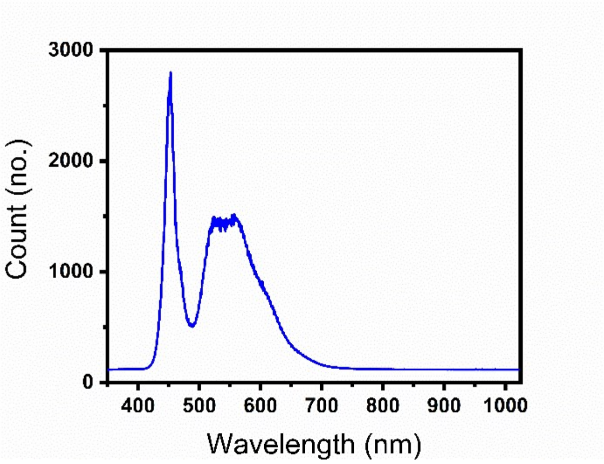

Figure S21. The emission spectrum of the white LED light source. Data obtained in the dark, utilizing a USB2000 Ocean Optics Spectrometer with an integration time of 5 ms, averaging over 1000 times.

Supplementary Tables

Table S1. Parameters used in the finite layer BET line of best fit. Method of fitting explained in the Supplementary Methods.

	Monolayer coverage per gram of material, n_m^{σ}/g (mol g^{-1})	**Net energy of desorption, $E_d - E_v$ (KJ mol^{-1})**	**Number of maximum layers, ν (no.)**
Data at 296 K	0.005	10.644	4.2

Table S2. XPS atomic percentages obtained for Cu-melanin thin films. For comparison, the range of values expected for neat melanin thin films based upon starting monomers are also shown. Data compliments Figure 4B.

Sample	**O 1s, (%)**	**C 1s, (%)**	**N 1s, (%)**	**Cu 2p, (%)**	**Cl 2p, (%)**
Neat melanin	18-29	64-72	7-9	-	-
1 min Cu- melanin film	18.0	71.0	10.8	0.25	0.03
2 min Cu- melanin film	18.1	70.4	10.8	0.54	0.15
5 min Cu- melanin film	18.2	70.8	10.1	0.66	0.31

Table S3. Cu(II) concentration of Cu-melanin supernatants measured using CW-EPR. The final concentrations were determined from the EPR standard Cu(II) solutions. The low Cu(II) concentration remaining in the Cu-melanin supernatant indicates the majority of Cu(II) added to melanin was incorporated into the final powder sample.

Starting Cu(II) (mol $g^{-1)}$	**Starting Cu(II) (mol ml^{-1})**	**Final Cu(II) in Supernatant (mol ml^{-1})**	**Final Cu(II) (based on supernatant (mol g^{-1})**	**Final Cu(II) (based on powder spectra) (mol g^{-1})**	**% of Cu(II) in melanin reduced to Cu(I)**
5×10^{-5}	5×10^{-6}	Noise	-	5×10^{-4}	-
5×10^{-4}	1×10^{-4}	4×10^{-5}	3×10^{-4}	8×10^{-5}	73%

Supplementary Methods

Adsorption isotherm: The determination of water adsorption behavior was performed according to previously published methods.[S3] In brief, a vacuum microbalance (CI Electronics Ltd.) was attached to a vapor delivery system in which vapor was introduced from a flask containing H_2O (deionized, Millipore) that had been degassed with three freeze−pump−thaw cycles. Pressure measurements were performed with a calibrated BOC-Edwards GK series, 0−50 mbar gauge, and rotary pumps were used to create a vacuum. The dry mass was obtained by pumping down on the sample overnight until the mass measured was constant. For adsorption measurements as a function of relative pressure (akin to relative humidity), the desired pressure of H_2O was admitted into the system, and the reservoir was closed off. The sample was allowed to equilibrate for at least 4 hours while the sample mass was monitored with the microbalance. For the next data point, the sample was dried by again pumping down overnight to obtain the dry weight. The pressure was then increased again and equilibrium achieved after approximately 2 hours, until the mass measured remained constant for at least 10 minutes. The same procedure was the repeated with increasing water vapor pressure. The saturation vapor pressure was obtained by opening the water reservoir and measuring the pressure directly (measured as 24.0 ± 0.1 mbar). Experiments were conducted at a constant temperature of 21.0 ± 0.5 °C.

The sample used was a 0.5 mmol g^{-1} sample, the same as the conductivity samples used in Figure 2A.

Data between 0.05 – 0.3 relative pressure was initially analyzed by using the linearized infinite layer BET equation:[S1]

$$\frac{p}{n^{\sigma}(p^{0}-p)}=\frac{1}{Zn_{m}^{\sigma}}+\frac{Z-1\,p}{Zn_{m}^{\sigma}p^{0}} \tag{S1}$$

where p is the vapor pressure of the adsorbate, p^{0} is the saturation vapour pressure of the adsorbate, n^{σ} is the number of moles adsorbed, n_{m}^{σ} is the number of moles required for monolayer coverage and

$$Z\approx e^{(E_{d}-E_{v})/RT} \tag{S2}$$

where E_{d} is the energy of adsorption, E_{v} is the energy of vaporisation, R is the universal gas constant and T is temperature. The linearised data enables the extraction of n_{m}^{σ} and $E_{d}-E_{v}$. Once the parameters have been extracted, the finite layer BET equation was used:

$$\frac{n^{\sigma}}{n_{m}^{\sigma}}=\frac{ZX}{1-X}\frac{1-(v+1)X^{v}+vX^{v+1}}{1+(Z-1)X-ZX^{v+1}} \tag{S3}$$

where v is the maximum number of monolayers and $X=\frac{p}{p^{0}}$.

UV-Vis absorbance: Data was obtained utilizing a UV-Vis-NIR Spectrophotometer 5000 (Varian) with Cary WinUV (Agilent Technologies) software. All absorbances were measured against a clear glass slide which acted as a baseline. Preparation of slides were as described in the Experimental Section. Thicknesses of any formed films were measured using a Dektak XT (Bruker). Using a sharp needle, three scratches were made on each sample to check the film homogeneity. Vision 64 software was used to control the machine stylus and collect the data. The length of each run was 400 µm, the duration of each run 8 sec and the stylus force 3 mg.

AFM: Samples prepared on glass slides as discussed in the Experimental Section. The AFM utilized was an Asylum Cypher High Resolution using tapping mode. The cantilevers (Budget Sensors) used for imaging had a resonant frequency of 75 kHz and a force constant of 3 N/m. All experiments were carried out under ambient conditions. Asylum Research software was used to collect and analyze the data. Data was obtained as a function of scan window size, i.e. image dimension, for each kind of film.

For samples prepared on other substrates, melanin was spin coated using the same recipes as per Experimental Section, but on mica, grade V-1 (ProSciTech); silicon wafers, (111)-orientation p-type with native oxide formed on the surface and surface resistance of 1-30 Ohm (ProSciTech) and silicon wafers with Si_3N_4 top layer (MMRC). Both types of silicon substrates and glass slides were pre-cleaned as described in the Experimental Section to increase the hydrophilicity of the surface and improve the quality of the films. The top layer of the mica substrates was peeled off, and melanin solution was spin coated immediately without any further treatment of the surface. Different substrates were selected to see whether the melanin thin film morphology and roughness was substrate dependent.

EPR: Cu(II) Glycine Standard Powders: Anhydrous $CuCl_2$ was prepared by drying $CuCl_2$ dihydrate salt (Sigma-Aldrich). A portion of the anhydrous $CuCl_2$ was immediately weighed out and dissolved into milli-Q water to make a stock solution of known Cu(II) concentration. A glycine stock solution was made from glycine powder. Different concentrations of $CuCl_2$ and glycine solutions were mixed according to the concentrations of Cu(II) used to prepare the Cu-melanin samples described in the main manuscript, which were then dried to extract the powder. The mixture was dried further under vacuum overnight and ground into a fine powder. The powders were dried again at 100°C for 1 hour before weighing. A test was done with weighing before and after exposure to ambient conditions overnight with no significant weight change detected. Furthermore, CW-EPR spectra of the copper glycine powders re-measured after a month of storage on the laboratory bench showed no change in EPR signal intensity. This indicates all the Cu(II) was bound to glycine and minimal moisture was absorbed from the laboratory.

EPR, Sample Preparation for Determining Cu(II)/Cu(I) Concentration: Cu-melanin powder samples were dried in an oven overnight at 60°C, then immediately transferred into a glove box. The powders were weighed into NMR sample tubes and sealed before transferring out of the glove box. Standard NMR tubes were used because the readily available NMR tubes had a wider diameter (0.5 cm) and shorter length (10 cm), which made transfer in a glovebox easier. The samples were measured with CW-EPR within 2 hours of being transferred out of the glove box. The CW-EPR spectra of the dried Cu-melanin samples resembled the CW-EPR line shape of the same samples measured under vacuum, indicating the samples transferred from the glove box were sufficiently sealed and measured dry. The spectrometer parameters are as below.

EPR, Operation for standard samples testing: X-band CW-EPR spectra of the dried Cu-melanin powders were measured with a Bruker Elexsys E-540 spectrometer. A Bruker ER 4105DR double resonator was used to correct for differences in the Q-factor between different loaded samples. A standard reference sample (Bruker strong pitch 0112S118) was placed in one cavity of the resonator for the duration of the experiment. The Cu-melanin and Cu glycine powders were measured in the other cavity. Prior to measurements, the volume in the microwave cavity was determined for where the magnetic field is homogenous. Samples were loaded to a level commensurate with the homogenous magnetic field. The other parameters for the spectrometer were as reported in the experimental section of the main manuscript.

EPR, Data Treatment of the Standard Calibration: The CW-EPR spectra were baseline corrected and filtered with a moving average filter using 5 neighboring data points. First, the melanin radical component of the Cu-melanin samples were baseline corrected, double integrated, and then subtracted from the double integral of the entire Cu-melanin spectrum, leaving the double integral associated with the Cu(II). The Cu(II) double integral was then divided by the mass of dried Cu-melanin powder to factor out differences in the mass of each sample, resulting in a relative spin concentration. The relative spin concentrations of the Cu glycine powders were determined in a similar manner. Integrals were calculated numerically by using the cumulative trapezoidal method.

To compare the double integrals of Cu-melanin powders (D_{SN}*) to the Cu glycine powders, small variations in the Q-factor of the double resonator (Q_S) were corrected with the standard reference sample (R). A change in the double integral of the reference sample (D_R) with a different loaded Cu sample is proportional to the change in the Q-factor of the double resonator (Q_S). The double integrals were corrected by applying the change in Q-factor from the first Cu sample measured (R1). For sample number N, with an uncalibrated double integral (D_{SN}):

$$Q_{SN} = \frac{D_{RN}}{D_{R1}} \tag{S4}$$

$$D_{SN}^{*} = Q_{SN} D_{SN} \tag{S5}$$

The total uncertainty was determined as ~15%: Due to small deviations from linearity in the Cu(II) standard powders used up to ~8%; Variance in the CW EPR signal measurements from switching samples in and out of the resonator (~5%); And from subtracting the melanin CW EPR signal from the Cu-melanin spectrum (~2%).

EPR, Determining Cu(I) Concentration in Cu-melanin Powders: A Cu-melanin powder made with 0.5 mmol g^{-1} was dissolved in aqueous ammonia, which served as a Cu(I) oxidizing agent, and a Cu(II) ligand. Cu(I) is highly unstable in aqueous solutions and will oxidize to Cu(II) due to the higher hydration energy of Cu(II) ions.[S4] Although a basic solution is required to dissolve melanin, an insoluble Cu(II) hydroxide complex can form. However, this problem can be overcome by using excess ammonia. A low concentration of aqueous ammonia mixed with Cu-melanin powder will initially produce a portion of insoluble Cu(II) hydroxide.[S4] Additional ammonia will then exchange with the hydroxide and form a soluble Cu(II) ammonia complex.[S4] Using 3 ml of ammonia solution (5 M) to dissolve 10 mg of Cu-melanin powder resulted in a non-viscous, homogeneous solution.

Supplementary Discussion

Adsorption Isotherm

The data presented in Figure S1 indicates that Cu-melanin adsorbs water that can be described by a pseudo type-2 isotherm,[S1, S3] i.e. a type 2 isotherm with finite number of water layers on the internal surface of the sample. The main difference between Cu-melanin and melanin adsorption isotherms[S3] is the magnitude of the water amounts adsorbed. Cu-melanin adsorbs a greater amount of water at low water vapor pressures compared to melanin. It then levels out and maintains the same gradient of increase, but with an offset that leads to higher water contents. In short, the data indicates Cu-melanin is more hydrophilic than standard synthetic melanin.

Photo EPR time traces.

Inspecting Figure S17 it can be seen that a positive photo EPR signal is clearly seen even in the dry material and is indeed greater than for the wetter samples. Then as can be seen the signal becomes attenuated with increasing hydration. This attenuation is due to a combination of the number of species generated being limited to the surface area and that the amount of semiquinones that can be generated becoming limited as the sample is being wetted.[5]

The opposite effect is seen for the Cu ⊥ features and essentially mirrors the melanin peak behavior.

Supplementary References

[S1] G. Barnes, I. Gentle, *Interfacial Science: An Introduction*, Oxford University Press, **2011**.
[S2] P. Meredith, T. Sarna, Pigment Cell Research **2006**, 19, 572.
[S3] A. B. Mostert, K. J. P. Davy, J. L. Ruggles, B. J. Powell, I. R. Gentle, P. Meredith, Langmuir **2010**, 26, 412.
[S4] B. Moody, *Comparative Inorganic Chemistry*, Elsevier, **2013**.
[S5] A. B. Mostert, S. B. Rienecker, C. Noble, G. R. Hanson, P. Meredith, Science Advances **2018**, 4, eaaq1293.